


Activating mitofusins interrupts mitochondrial degeneration and delays disease progression in SOD1 mutant amyotrophic lateral sclerosis

Xiawei Dang ^{1,2}, Lihong Zhang¹, Antonietta Franco¹ and Gerald W. Dorn II^{1,*}

¹Department of Internal Medicine, Washington University School of Medicine, St. Louis MO USA

²Department of Psychiatry, The First Affiliated Hospital of Xi'an Jiao Tong University, Xi'an, Shaanxi 710061, China

*To whom correspondence should be addressed at: Washington University Center for Pharmacogenomics, 660 S Euclid Ave., Campus Box 8220, St. Louis, MO 63110, USA. Tel: +1 314 362-4892. Fax: +1 314 362-8844; Email: gdorn@wustl.edu

Abstract

Mitochondrial involvement in neurodegenerative diseases is widespread and multifactorial. Targeting mitochondrial pathology is therefore of interest. The recent development of bioactive molecules that modulate mitochondrial dynamics (fusion, fission and motility) offers a new therapeutic approach for neurodegenerative diseases with either indirect or direct mitochondrial involvement. Here, we asked: (1) Can enhanced mitochondrial fusion and motility improve secondary mitochondrial pathology in superoxide dismutase1 (SOD1) mutant amyotrophic lateral sclerosis (ALS)? And: (2) What is the impact of enhancing mitochondria fitness on *in vivo* manifestations of SOD1 mutant ALS? We observed that small molecule mitofusin activators corrected mitochondrial fragmentation, depolarization and dysmotility in genetically diverse ALS patient reprogrammed motor neurons and fibroblasts, and in motor neurons, sensory neurons and fibroblasts from SOD1 G93A mice. Continuous, but not intermittent, pharmacologic mitofusin activation delayed phenotype progression and lethality in SOD1 G93A mice, reducing neuron loss and improving neuromuscular connectivity. Mechanistically, mitofusin activation increased mitochondrial motility, fitness and residency within neuromuscular synapses; reduced mitochondrial reactive oxygen species production; and diminished apoptosis in SOD1 mutant neurons. These benefits were accompanied by improved mitochondrial respiratory coupling, despite characteristic SOD1 mutant ALS-associated downregulation of mitochondrial respiratory complexes. Targeting mitochondrial dysdynamism is a promising approach to alleviate pathology caused by secondary mitochondrial dysfunction in some neurodegenerative diseases.

Introduction

Mitochondria support neuronal signaling, repair and regeneration by producing ATP. Abnormal mitochondrial morphology, transport and metabolism are reported in numerous etiologically diverse neurodegenerative diseases (1–3). In most of these conditions mitochondrial phenotypes are secondary events evoked by a variety of primary non-mitochondrial abnormalities. The pathophysiological impact of mitochondrial dysfunction on the progression of these non-mitochondrial neurodegenerative diseases is uncertain.

One of the most intensively studied neurodegenerative diseases manifesting secondary mitochondrial abnormalities is the rare genetic form of familial amyotrophic lateral sclerosis (ALS) caused by over 200 different mutations of the SOD1 gene encoding cytoplasmic Cu, Zn and superoxide dismutase (SOD) (4,5) (<https://alsod.ac.uk/output/gene.php/SOD1>). Mitochondria in this condition have been described as fragmented, hypomotile and/or metabolically impaired (6–9). Multiple proposed mechanisms link mutant SOD1 to mitochondrial damage, including atypical mitochondrial bioenergetics or calcium signaling, increased oxidative stress or apoptosis, reduced axonal transport and an imbalance in mitochondrial fission/fusion (10,11). At the molecular level, misfolded mutant SOD1 proteins may interact and interfere with

both neuronal mitochondria (12–14) and the axonal transport apparatus responsible for mitochondrial motility (15).

Mitochondria-targeted interventions have been proposed for ALS and other neurodegenerative diseases (11,16,17), but there are few available options: The cell penetrant peptides SS-31 (Elamipretide) that targets cardiolipin to enhance mitochondrial respiration (18) and P110 that suppresses disease-associated hyperactivity of the mitochondrial fission factor DRP-1 (19) each reportedly delay progression of neuromuscular degeneration in the SOD1 G93A mouse model of ALS (20,21). These findings support efforts to expand the repertoire of available mitochondria-targeted therapeutics and evaluate novel mechanistic approaches for mitochondrial-directed therapeutics in SOD1 mutant ALS.

Mitochondrial fusion is a central determinant of organelle morphology and, by promoting mitochondrial repair via content exchange and genome complementation, is necessary for normal mitochondrial respiratory function (22). Mitofusin (MFN)1 and MFN2 mediate the initial events in mitochondrial fusion by physically tethering adjacent organelles and merging their outer mitochondrial membranes (23,24). Accordingly, MFN2 mutations cause the human peripheral neuropathy Charcot-Marie-Tooth disease type 2A (CMT2A) in which impaired mitochondrial fusion results in their fragmentation and loss of polarization (25,26)

and depressed mitochondrial motility suppresses their transport through neuronal axons (27–30). The process by which MFNs mediate mitochondrial fusion has been thoroughly described (22), and their regulatory role in mitochondrial transport is posited to involve interactions with the Miro/Milton mitochondrial transport protein complex (31,32). Thus, MFNs play central modulatory roles in mitochondrial fusion and transport within neurons, which are abnormal in SOD1 mutant ALS. Moreover, MFNs regulate mitochondria-endoplasmic reticular tethering, reactive oxygen species (ROS) production and oxidative phosphorylation (33–35) that can contribute to ALS. Accordingly, we asked if increasing MFN activity in SOD1 ALS could improve these characteristic mitochondrial abnormalities. We further asked whether correcting SOD1 ALS mitochondrial phenotypes would meaningfully impact *in vivo* neuromuscular degeneration.

Here, using primary ALS patient dermal fibroblasts and directly reprogrammed motor neurons we defined mitochondrial abnormalities in SOD1 mutant ALS at baseline and after allosteric MFN activation. Then, using the well-characterized SOD1 G93A mutant mouse model of aggressive ALS (36,37) we determined that this purely mitochondria-directed intervention can delay functional neuromuscular degeneration. Mechanistically, MFN activation improved mitochondrial respiration, reduced oxidant stress and suppressed neuronal apoptosis. These findings further establish a role for mitochondrial dynamic dysfunction in neuromuscular disease caused by SOD1 mutants and suggest that mitochondria-targeted therapeutics, while by no means curative, can be disease-modifying.

Results

Mitochondrial dysmorphology and depolarization are severe in SOD1 mutant ALS patient fibroblasts and are improved by MFN activation

Recent studies have shown that cultured primary human dermal fibroblasts can be induced to recapitulate characteristic *in vivo* disease-related mitochondrial phenotypes for some genetic neurodegenerative conditions (26,38). It is not known if this approach, in which galactose is substituted for glucose in the culture medium to promote oxidative metabolism (39,40), will also evoke mitochondrial phenotypes in genetic ALS. Here, live-cell imaging of mitochondria within primary fibroblasts from ALS patients carrying three different ALS SOD1 mutations (L38V, I113T and L145F), the ALS FUS R521G mutation and the ALS TDP43 A382T mutation appeared normal under standard culture conditions (Supplementary Material, Fig. S1). However, mitochondrial fragmentation (reduced aspect ratio [length/width], which reflects the balance between mitochondrial fission and fusion (41)) and depolarization (which reflects loss of respiratory function (42)) were observed in most cells after culturing in galactose medium (Supplementary Material, Fig. S1). Morphological and functional abnormalities of galactose-fed fibroblast mitochondria were most severe in ALS caused by SOD1 gene mutations (Fig. 1), whereas mitochondria of TDP43 A382T fibroblasts appeared normal (Fig. 1). The prototype small molecule MFN activator Chimera C (compound 2 in reference (43); 100 nM, 48 h) (43,44) improved mitochondrial fragmentation and loss of polarization in each of the ALS cell lines manifesting disease-associated abnormalities (Fig. 1). As previously reported (43), Chimera C had no effect on mitochondria of normal subject fibroblasts (Fig. 1).

Mitochondrial dysmotility in SOD1 mutant reprogrammed motor neurons is similar to other genetic forms of ALS and improves after MFN activation

The observation that metabolic stress provokes pathological mitochondrial phenotypes in SOD1 mutant ALS dermal fibroblasts reveals widespread mitochondrial involvement in this condition, even though the disease selectively affects upper and lower motor neurons (11). However, morphological and respiratory abnormalities represent only a portion of the spectrum of mitochondrial dysfunction reported in ALS; mitochondrial dysmotility may also play a role and is likely most important in long neuronal processes, relative to compact cells like fibroblasts (8,9). For this reason, we employed direct microRNA-mediated conversion (29,45) to generate motor neurons from ALS patient fibroblasts lines and interrogated mitochondrial motility within neuronal processes; reprogrammed motor neurons from three normal subjects served as controls. Reprogramming efficiency of ALS patient fibroblasts to neurons was ~90%, with ~80% of reprogrammed neurons staining positively for motor neuron-specific HB9/MNX1 (Fig. 2A). For unknown reasons, SOD1 L145F cells did not survive repeated attempts at neuronal reprogramming and were therefore not studied as motor neurons.

Mitochondrial dysmotility in motor neuron processes was a consistent finding across all four reprogrammed ALS mutant lines (SOD1 L38V and I113T, FUS R521G and TDP43 A382T) (Fig. 2B). As in the parental ALS patient fibroblast lines, mitochondria of SOD1 mutant neurons exhibited greater mitochondrial fragmentation (i.e. lower aspect ratio) and depolarization than mitochondria from FUS and TDP43 mutant neurons (Fig. 2C and D). Nevertheless, MFN activation with Chimera C (100 nM, 48 h) improved mitochondrial transport, aspect ratio and polarization status in each ALS motor neuron line. The magnitude of response to MFN activation was generally proportional to the degree of baseline abnormality, i.e. greater benefit accrued to neurons manifesting the most severe anomalies.

Sustained, but not transient, MFN activation delays ALS in SOD1G93A mice

Together, the above studies support the proposition that mitochondrial defects in SOD1 mutant ALS neurons and fibroblasts can be improved by pharmacological MFN activation. Accordingly, we asked if targeting mitochondrial fusion and motility in this manner is sufficient to mitigate neuromuscular degeneration caused by mutant SOD1 *in vivo*. SOD1 G93A transgenic mice are a well-characterized murine model of aggressive ALS in which G93A mutant human SOD1 is expressed at high levels under control of the native human SOD1 gene promoter (36). While SOD1 G93A was not one of the SOD1 mutant ALS patient lines we were able to access for *in vitro* studies, Chimera C effects on mitochondrial defects in the ALS cell lines appeared agnostic to specific cell mutation. Therefore, we performed a randomized blinded trial of MFN activation in SOD1 G93A ALS mice. Because Chimera C exhibits nearly complete first-pass hepatic clearance (43), we used an equipotent MFN activator previously validated *in vivo*, MiM111 (compound 13B in reference (43) and compound 2 in reference (46)) (29,43,46), for studies in mice. MFN activation with MiM111 (30 mg/kg IM once daily (29)) or its vehicle was initiated in 60-day-old SOD1 G93A mice after baseline evaluation of neuromuscular function and neuroelectrophysiological testing. This corresponds to an early stage of the progressive ALS-like phenotype when some metrics of neuromuscular dysfunction

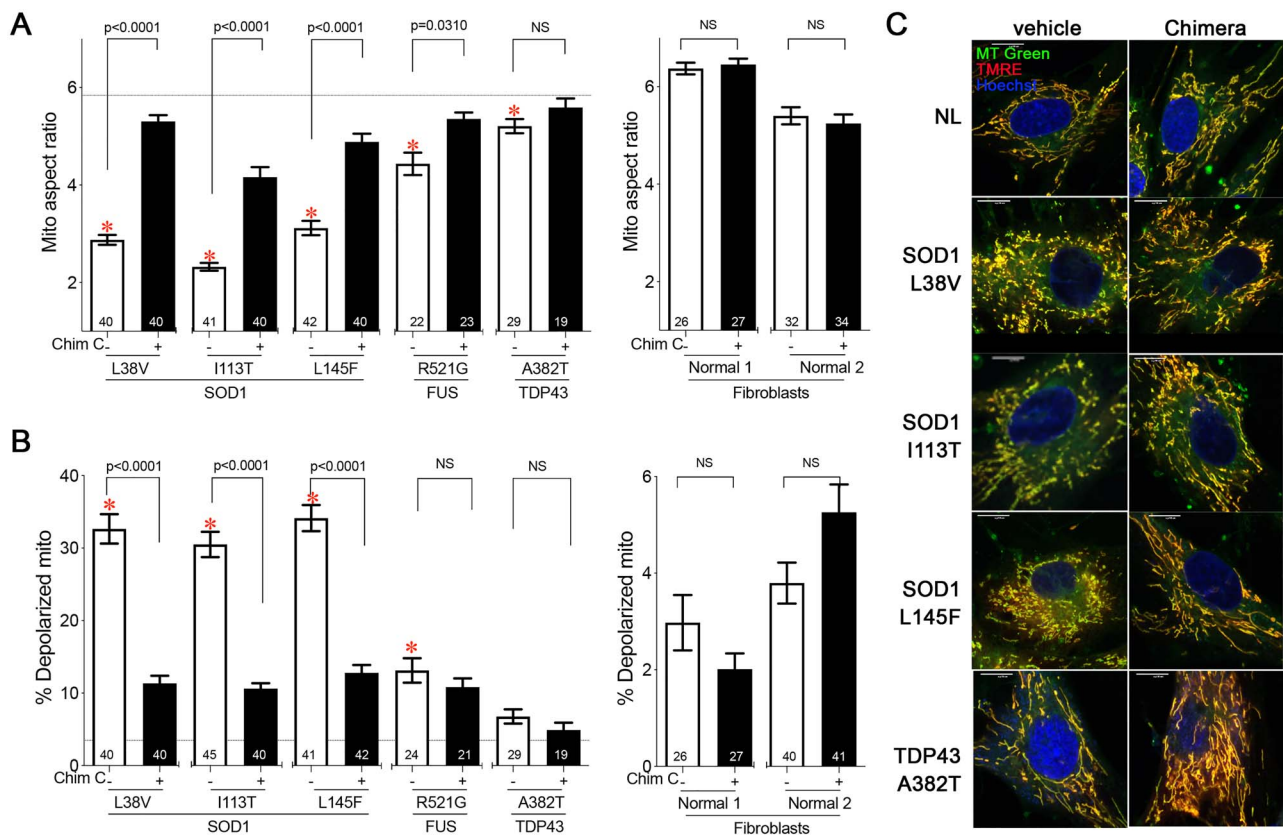


Figure 1. Mitochondrial phenotypes in normal and ALS patient primary dermal fibroblasts and their response to mitofusin activation. Mitochondrial aspect ratio (length/width; **A**) and loss of polarization/respiratory function (**B**) in galactose-fed human fibroblasts. * = $P < 0.05$ vs normal controls (shown in right hand bar graphs and as horizontal dashed line in ALS graphs); P values are response to mitofusin activator Chimera C (Chim C) 100 nM added 48 h prior to study. Results are mean \pm SEM; statistics by ANOVA. Number of cells evaluated per group is indicated at the base of bars in graphs. (**C**) Representative confocal images.

are already mildly diminished (Supplementary Material, Fig. S2). Surprisingly, MiM111 administration at the same dose, route and dosing interval that normalized full-blown murine CMT2A (29) did not meaningfully alter phenotype progression in SOD1 G93A mice (Supplementary Material, Fig. S3).

We considered possible explanations for the failure of MFN activation with MiM111 to alter phenotype progression in SOD1 G93A mice: (1) If mitochondrial pathology is a secondary event in SOD1 ALS with little impact on neuromuscular degeneration, then its correction through MFN activation would not alter the disease. (2) Our reasoning about mutation agnosticism might be erroneous and SOD1 G93A might not respond to MFN activation as robustly as the SOD1 mutations we had studied *in vitro*. (3) Transient or 'burst' MFN activation with short-acting MiM111 (29) might not reproduce our *in vitro* experiments, in which Chimera C in the culture media provided continuous MFN activation. We recognized that these possibilities could be tested by performing a parallel SOD1 G93A mouse study employing the newly described and equipotent longer-lasting MFN activator, N-(4-hydroxycyclohexyl)-2-(3-phenylpropyl) cyclopropane-1-carboxamide (here designated CPR1; compound 5 in reference (46)). Accordingly, we randomized fresh cohorts of 60-day-old SOD1 G93A mice to treatment with CPR1 (60 mg/kg twice daily by oral gavage) or vehicle (10% DMSO/90% [30% HB- β -CD]) after baseline phenotype evaluation. Pharmacokinetic and pharmacodynamic studies of CPR1 indicated that this twice daily oral CPR1 dosing regimen would provide continuous, sustained MFN activation (Supplementary Material, Fig. S4) (46).

We employed a combined test that integrates results of ledge testing, hindlimb clasp, gait abnormalities and kyphosis to score neuromuscular dysfunction (47). Using this system, a score of 0 is normal and 12 equates to paralysis; our predetermined criterion for study termination and euthanasia was loss of mobility sufficient for independent viability, which typically reflects a combined score of 8 or greater. CPR1 administration decreased the rate at which neuromuscular function declined: The time from disease onset to the pre-terminal state (defined as the interval between dysfunction score 1 and score 6) was increased in CPR1 treated mice by 43%, from 49 ± 3 days (veh) to 70 ± 4 days (CPR1; $P = 0.0006$ by t-test). Delayed phenotype progression in CPR1-treated SOD1 G93A mice was further evident in serial measurements of RotaRod latency (time to falling off a slowly accelerating elevated rotating cylinder; Fig. 3A), deterioration of grip strength (time to falling from an elevated inverted screen; Fig. 3B) and the neuromuscular dysfunction score (Fig. 3C). The ages at which metrics of neuromuscular function declined by 50% were increased in CPR1-treated mice by 48% for RotaRod testing (94–139 days), 23% for grip strength (98–121 days) and 28% for the combined functional score (103–132 days). Divergence in the deterioration time courses for grip time and neuromuscular dysfunction scores between vehicle- and CPR1-treated mice suggested that some benefits of MFN activation accrued throughout the observation period (Fig. 3B and C).

Neuromuscular integrity in clinical ALS can be objectively assessed with neuro-electrophysiological ('nerve conduction')

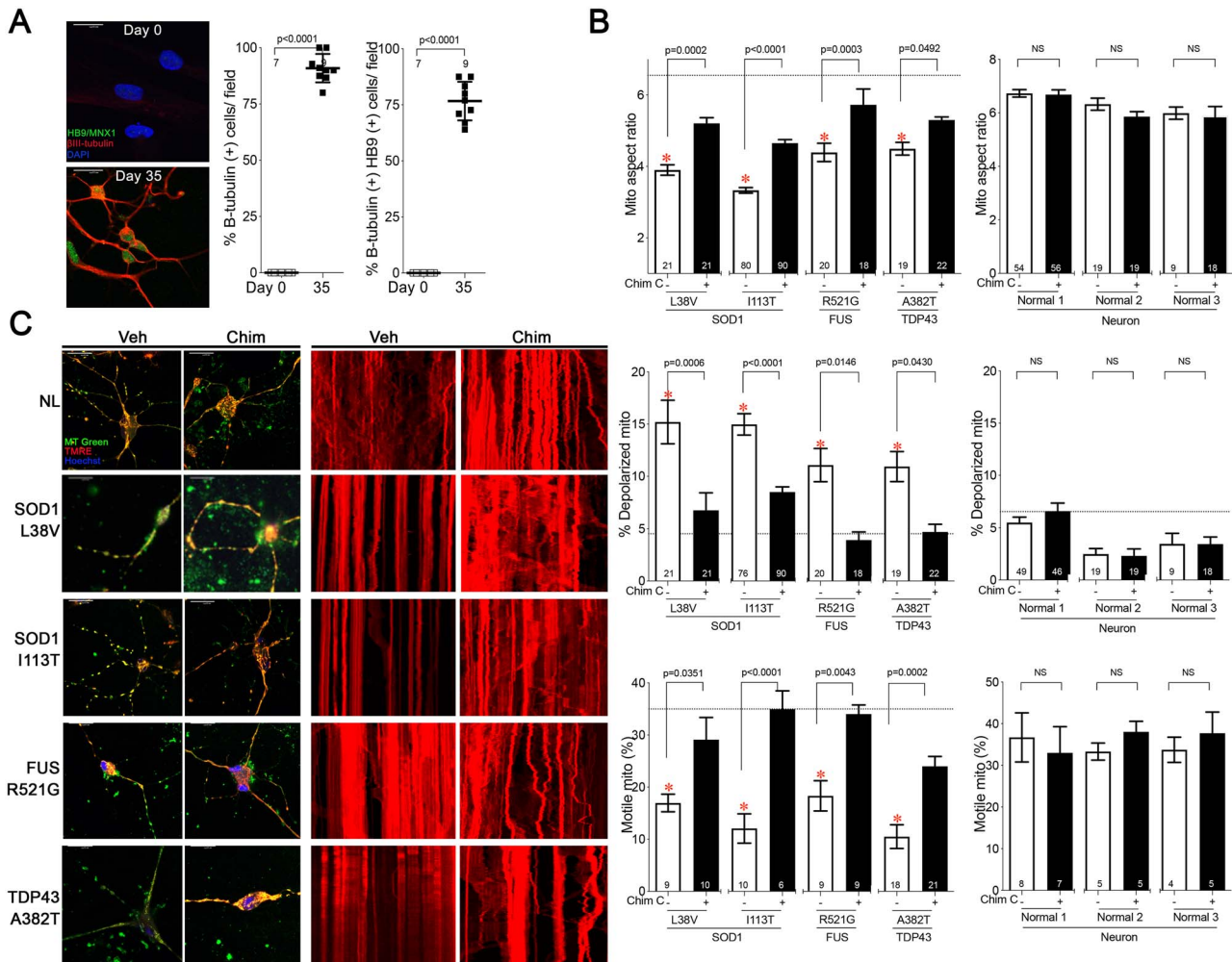


Figure 2. Mitochondrial phenotypes in normal and ALS patient reprogrammed motor neurons and their response to mitofusin activation. (A) Immunostaining of parental SOD1 I113T fibroblasts (top) and reprogrammed neurons (bottom). Neuronal axons and soma stain positive for β -III-tubulin (red) and motor neuron nuclei stain positive for HB9/MNX1 (green). Group quantitative data are to the right; each marker represents a different microscopic field containing at least five cells from two independent reprogramming studies. *P* values used unpaired *t*-test. (B) Mitochondrial aspect ratio (top), loss of polarization (middle) and % motile mitochondria (bottom). Numbers of cells from at least three independent experiments/reprogramming events are shown on bars. Chim C = mitofusin activator (Chimera, 100 nM) added 48 h prior to study; * = *P* < 0.05 vs normal control (horizontal dashed line and right graphs). Results are mean \pm SEM; *P* values used ANOVA. (C) Representative confocal images (left) and mitochondrial motility kymographs (right).

testing (48). Here, sequential neuro-electrophysiological testing of SOD1 G93A mice (Fig. 3D) showed that MFN activation with CPR1 delayed the characteristic loss of compound muscle action potential (CMAP) amplitude by 23% (point of 50% decline was extended from 97 to 119 days), and latency prolongation (i.e. decreased nerve conduction velocity) by 60% (point of 50% decline was extended from 77 to 123 days).

Early mortality from the sequelae of denervation myoatrophy is a hallmark of human ALS and the SOD1 G93A mouse. CPR1 treatment prolonged survival of SOD1 G93A mice by 10%, from 150 \pm 4 days (veh: median 153 days, 95% CI: 129–174) to 165 \pm 2 days (CPR1: median 163 days, 95% CI: 157–179; *P* = 0.002) (Fig. 3E). Because this mouse model can show more rapid phenotypic progression in males than females (49), neuromuscular function was analyzed independently by sex. CPR1 significantly delayed endpoints of phenotype progression in mice of both sexes (Supplementary Material, Fig. S5). Median survival in vehicle-treated female ALS mice was 155 days, which increased by 12% to 173.5 days with CPR1 treatment (*P* = 0.0027). Median survival in

vehicle-treated male ALS mice was 149.5 days, which increased by 10% to 157 days with CPR1 treatment (*P* = 0.021).

MFN activation corrects mitochondrial phenotypes in SOD1G93A motor neurons *in vitro* and *in vivo*

Positive *in vivo* results with CPR1 did not formally address the possibility that the SOD1 G93A mutation responds differently to MFN activation than SOD1 L38V and I113T mutations studied as ALS patient reprogrammed neurons (*vide supra*). Therefore, we cultured mouse spinal motor neurons (mSMN) from SOD1 G93A mouse embryos and evaluated *in vitro* and *in vivo* SOD1 G93A motor neuron responses to MFN activation. HB-9 and β -III tubulin co-staining confirmed that the cultured spinal cells were motor neurons (Fig. 4A).

Baseline mitochondrial abnormalities in SOD1 G93A mSMN were defined using the parameters measured in SOD1 mutant ALS patient reprogrammed motor neurons (see Fig. 2). As with

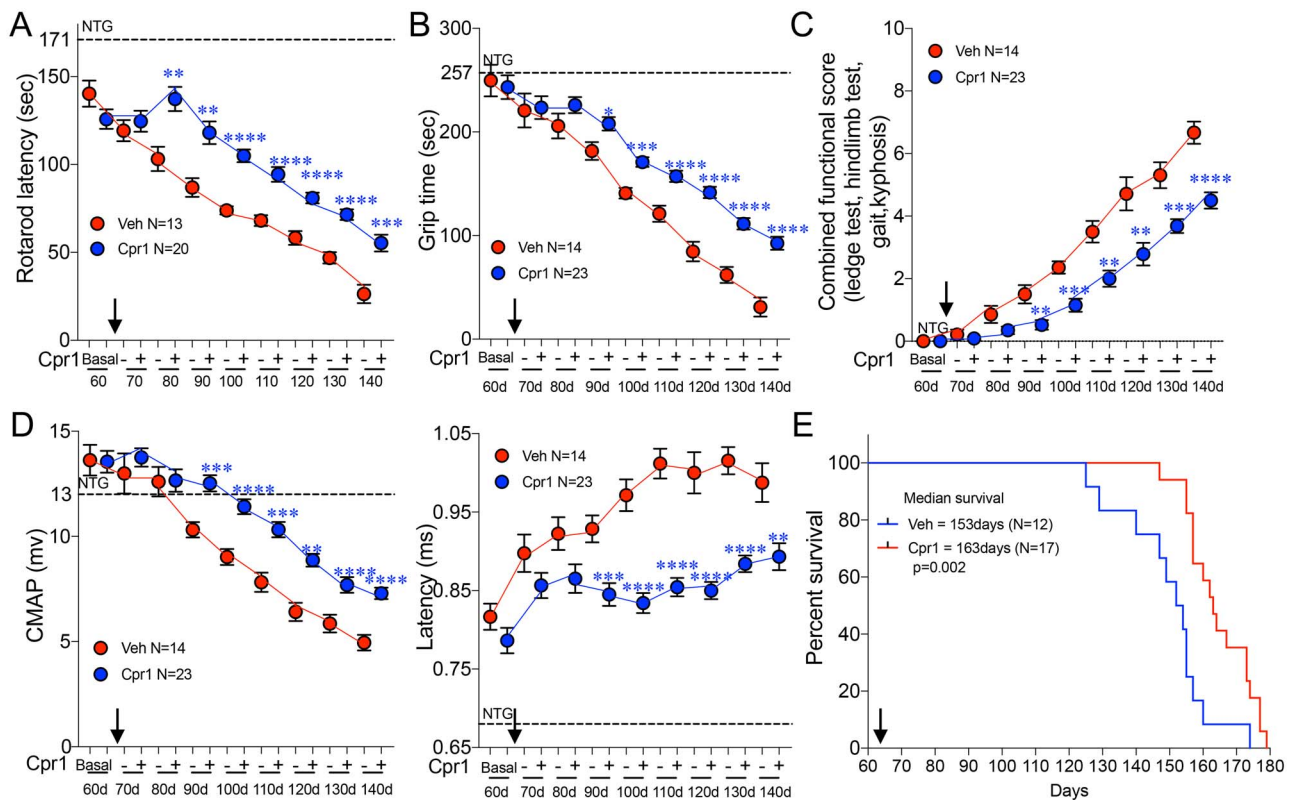


Figure 3. Sustained mitofusin activation delayed ALS phenotypes in SOD1 G93A ALS mice. (A) Rotarod latency. (B) Inverted grip time. (C) Neuromuscular dysfunction score. (D) Results of neuroelectrophysiology testing (left, CMAP amplitude; right, CMAP latency). (E) Survival. 'Basal' is pre-treatment; treatment was started at arrow. Horizontal axis is mouse age in days (d). Mean \pm SEM; * = $P < 0.05$, ** = $P < 0.01$, *** = $P < 0.001$, **** = $P < 0.0001$ vs veh (unpaired t-test). Horizontal dashed line represents mean value for nontransgenic (NTG) normal mice ($N = 5$), which did not change over time.

the patient-derived motor neurons, SOD1 G93A mSMN exhibited severe mitochondrial fragmentation, loss of polarization and hypomotility in comparison with normal (wild-type) mSMN (Fig. 4B–D). CPR1, which activates MFNs by the same allosteric mechanism and with an almost identical EC_{50} as Chimera C (46), corrected mitochondrial fragmentation, depolarization and dysmotility in a manner reproducing Chimera C effects on patient-derived SOD1 L38V and I113T mutant motor neurons (Fig. 4B–D; compare to Fig. 2).

The *in vivo* correlates for mitochondrial pathology in SOD1 ALS include reduced numbers of axonal mitochondria with structural degeneration and vacuolization of those that remain (6,50). Ultrastructural examination of 140-day-old SOD1 G93A mouse spinal cord ventral motor nuclei (not shown) and lower limb peripheral nerve axons recapitulated these findings in vehicle treated ALS mice, and revealed improved mitochondrial morphology with CPR1 treatment (Fig. 4E).

Mitochondrial motility through motor neurons is difficult to directly observe *in vivo*. We had demonstrated greater numbers of motile mitochondria in *ex vivo* sciatic nerve axons of SOD1 G93A after CPR1 treatment (see Supplementary Material, Fig. S4). As an *in vivo* correlate of disease responsiveness and mitochondrial motility, we reasoned that mitochondrial residency within distal synapses reflects their transport through neurons and delivery to neuromuscular junctions (NMJs). Indeed, both mitochondrial residency within synapses of lower limb gastrocnemius muscles and the number of those neuromuscular synapses were decreased in SOD1 G93A mice, and restored by CPR1-treatment (Fig. 4F). Taken together, our results demonstrate that MFN activation can improve neuronal mitochondrial abnormalities for multiple

human and murine SOD1 mutants *in vitro*, and within SOD1 G93A motor neurons *in vivo*.

Mitochondrial abnormalities in SOD1 G93A mice are not limited to motor neurons

Our results in human dermal fibroblasts (see Fig. 1) revealed that mitochondrial phenotypes in SOD1 mutant ALS are not specific to motor neurons (*vide supra*). To determine if mitochondrial pathology was also generalized in SOD1 G93A mutant mice, adult dorsal root ganglion (DRG) sensory neurons and embryonic fibroblasts (MEFs; galactose fed) were cultured from SOD1 G93A mice and interrogated using the same battery of mitochondrial tests. In both cell types mitochondrial fragmentation, loss of polarization and (for DRGs) dysmotility were present, and improved after MFN activation (Supplementary Material, Fig. S6). There were no meaningful differences in mitochondrial pathology or response to MFN activation between SOD1 G93A mouse motor and sensory neurons (compare Supplementary Material, Figs S6–S4B–D).

MFN activation protects SOD1 G93A neurons from apoptosis

Loss of motor neurons from mitochondrial pathway apoptosis is posited to contribute to neuromuscular degeneration in ALS (51,52). We considered that the reparative and restorative effects of MFN activation on neuronal mitochondria might delay phenotype progression in SOD1 G93A mice by reducing the apoptotic loss of motor neurons. Indeed, our earlier observation that CPR1-treated SOD1 G93A mice retained more neuromuscular synapses than their vehicle-treated counterparts (see Fig. 4F)

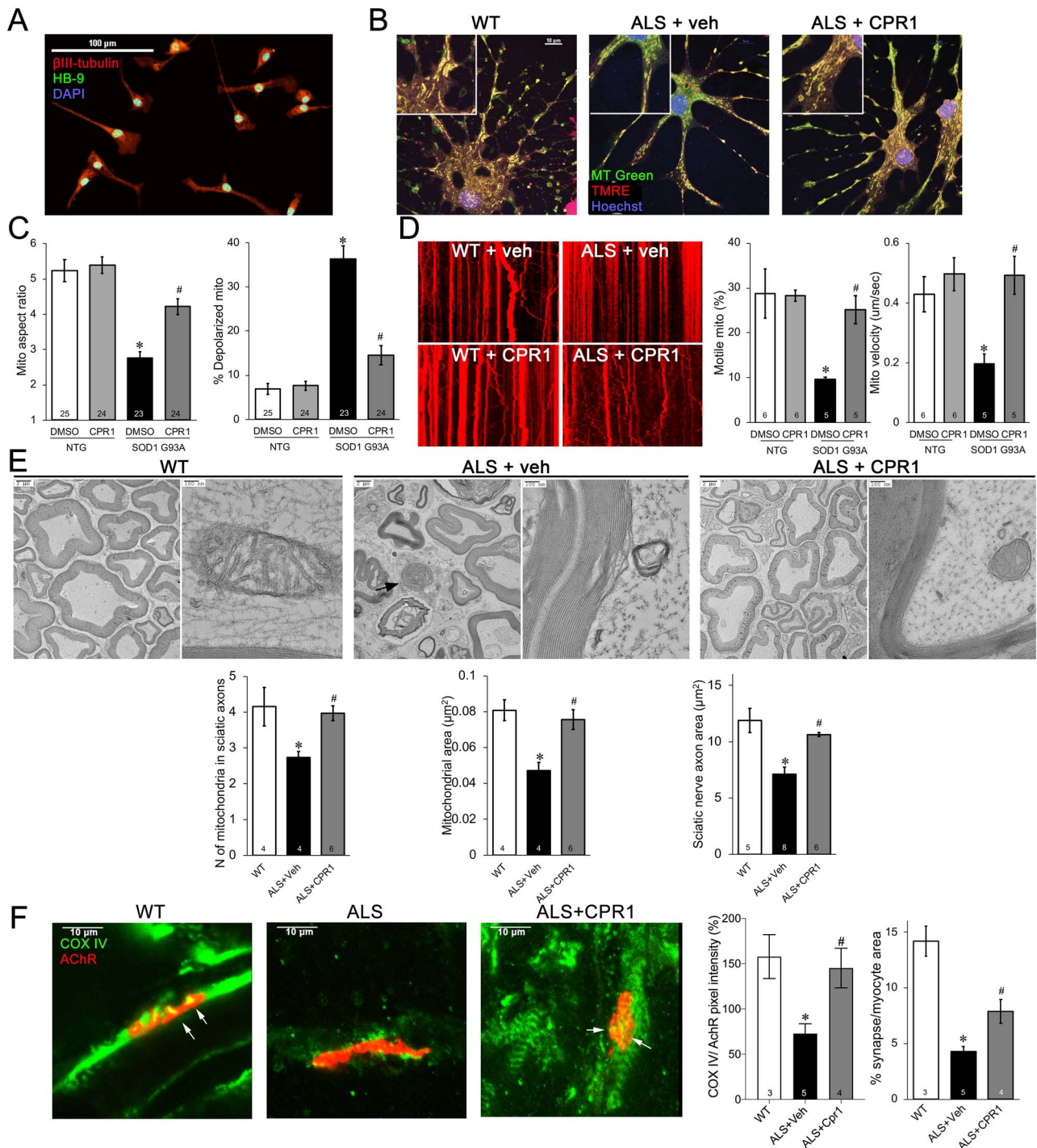


Figure 4. Mitofusin activation reverse mitochondrial phenotypes of SOD1 G93A mouse motor neurons *in vitro* and *in vivo*. (**A–D**) Results of studies with spinal motor neurons cultured from SOD1 G93A mouse embryos. (**A**) β -III-tubulin (red) immunostaining is a general neuron marker, whereas nuclear HB9/MNX1 (green) is specific for motor neurons. (**B**) Confocal images of wild-type (WT) and vehicle- or Chim-treated SOD1 G93A (ALS) neurons. Healthy mitochondria co-stain green (MT Green) and red (TMRE), appearing orange; functionally impaired depolarized mitochondria appear green (insets). (**C**) Group quantitative data for mitochondrial aspect ratio (left) and depolarization (right). (**D**) Results of mitochondrial motility studies. (left) Representative kymographic raw data; (right) quantitative group data. (**E, F**) Results of studies on SOD1 G93A mouse tissues. (**E**) Transmission electron microscopy of mid sciatic nerve (left panels, 2000x; right panels, 40000x). Arrow indicates myelin dense body of degenerated axon. Quantitative data are shown below. (**F**) Confocal micrographs of gastrocnemius neuromuscular junctions labeled red with anti-acetylcholine receptor (AChR); mitochondrial cytochrome oxidase (COX) IV is labeled green. Mitochondria within terminal synapses appear yellow (arrows). Quantitative data are to the right. Mean \pm SEM; * = $P < 0.05$ vs wild-type (WT/NTG) control; # = $P < 0.05$ vs vehicle-treated ALS (ALS) by ANOVA. Number of cells or mice evaluated per group is indicated at the base of bars in graphs.

supports the idea that MFN activation can confer some degree of neuroprotection.

As previously reported (53), neurons expressing SOD1 G93A exhibit increased TUNEL labeling, reflecting neuronal apoptosis. Here, TUNEL positivity of lumbar spine ventral horn motor neurons was increased in SOD1 G93A mice, and was reduced by CPR1 treatment (Fig. 5A). Likewise, increased TUNEL positivity in cultured SOD1 G93A mouse spinal motor (Fig. 5B) and DRG sensory neurons (Fig. 5C) was markedly reduced by MFN activation. Moreover, propidium iodide (PI) staining, which labels late apoptotic and necrotic cell nuclei, paralleled TUNEL labeling of mSMN and DRGs; the relative responses to MFN activation were also similar (Fig. 5B and C; PI positivity).

Uncoupling of mitochondrial respiration from ATP synthesis can form reactive oxygen species (ROS) as electrons are shunted to molecular oxygen and form superoxide. Independent of postulated toxic effects of misfolded SOD1 on mitochondria (54), dysfunction or deficiency of SOD1 can potentially increase neurotoxicity of elaborated ROS by interrupting superoxide conversion to hydrogen peroxide and water (55). Moreover, increased mitochondrial ROS elaboration by SOD1 G93A neurons is a potential mechanism for stimulating apoptosis (11,56). Therefore, we used MitoSOX staining to interrogate the effects of MFN activation on mitochondrial ROS elaboration in cultured mSMN and DRGs from SOD1 G93A mice. Both types of ALS neurons exhibited increased mitoROS levels, and each were moderated by MFN activation (Fig. 5B and C; MitoSOX). ROS suppression after MFN activation was not attributable to altered association of misfolded SOD1 G93A with mitochondria, which was not changed in CPR1-treated mouse brain (Supplementary Material, Fig. S7).

Accelerated neuronal growth/repair opposes, and can partially obviate, programmed neuronal death. Because MFN activation can stimulate neuron regeneration by improving delivery of mitochondria to terminal nerve growth buds (29), we probed the effects of MFN activation on mitochondrial residency within SOD1 G93A mSMN and DRG termini, and on neuronal outgrowth in tissue culture. The prevalence of mitochondria-occupied SOD1 G93A neuron termini was less than half that of normal wild-type neurons, but was normalized after MFN activation (Fig. 5B and C). Moreover, sluggish SOD1 G93A neuron outgrowth was restored to normal levels after MFN activation (Fig. 5B and C; axon intersections/cell).

MFN activation improves mitochondrial respiratory coupling in SOD1 G93A motor neurons

The above results and published studies suggested that MFN activation might moderate neuronal degeneration in SOD1 mutant ALS by improving mitochondrial respiratory fitness (7,57). To examine this notion we assayed expression of representative mitochondrial respiratory complex proteins in normal and ALS patient SOD1 mutant reprogrammed motor neurons. Compared to normal subject neurons, respiratory complex I–IV proteins were downregulated in SOD1 L38V and I113T motor neurons (Fig. 6A), whereas levels of complex V, MFN1 and MFN2 were unchanged (Fig. 6A and B). Importantly, MFN activation with CPR1 (100 nM, 48 h), which had restored mitochondrial morphology, polarization status, motility and ROS levels (see Figs 4 and 5), did not correct the loss of these electron transport chain proteins (Fig. 6A). By contrast, when mitochondrial respiration was assayed by Seahorse testing (58) of normal, SOD1 L38V and SOD1 I113T motor neurons, the characteristic ALS-associated decreases in basal and ATP-linked respiration (7,59,60) were reversed by MFN activation

with CPR1 (Fig. 6C). Consistent with not correcting respiratory chain protein levels, CPR1 did not restore maximal respiration (Fig. 6C). Thus, MFN activation of SOD1 mutant motor neurons improved functional coupling of oxygen consumption to ATP production, potentially enhancing regenerative capacity while simultaneously diminishing ROS mitotoxicity and apoptosis.

Discussion

There were two major scientific goals for this project. First, to understand whether a pharmacological intervention aimed purely at enhancing mitochondrial fusion and motility could alleviate the multiple mitochondrial abnormalities indirectly provoked by SOD1 mutations linked to juvenile ALS. And second, to determine if improving mitochondrial dysdynamism can mitigate neuromuscular phenotypes in an *in vivo* model of SOD1 mutant ALS. Our results are notable for demonstrating that mitochondrial abnormalities provoked by ALS-associated SOD1 mutations are not specific to motor neurons, or even to neurons in general, but are variably manifested in non-neuronal cells such as fibroblasts. And across the various neuronal and non-neuronal cell types studied, mutant SOD1-induced mitochondrial phenotypes were improved by MFN activation. Moreover, enhancing mitochondrial fusion and motility through MFN activation improved ATP-linked respiration and reduced mitochondrial ROS elaboration in SOD1 mutant neurons, which translated *in vivo* into neuronal retention and delayed functional neuromuscular deterioration. Although SOD1 mutant mouse survival was also significantly prolonged by MFN activation, the increase in longevity was proportionally less than attenuation of neuromuscular phenotypes. If one were to express these collective findings in clinical terms, MFN activation improved quality of life more than the quantity of life in this model.

Mitochondria support neural function by producing ATP for neuronal signaling, repair and regrowth. Mitochondrial fusion regulated by MFNs maintains respiratory fitness by restoring damaged mitochondria through content exchange and genome complementation (22). Loss of MFNs, as by gene ablation or expression of dysfunctional mutants, evokes mitochondrial dysfunction and induces senescent or degenerative cellular phenotypes in neuronal tissue, skeletal and cardiac muscle, and other tissues (25,29,61–67). The experiment of nature for MFN loss of function is CMT2A, a debilitating peripheral neuropathy caused by dozens of dominant suppressive MFN2 mutations (68–71). Murine models of CMT2A are improved by increasing MFN activity through transgenic MFN overexpression or pharmacological activation, apparently without adverse effects (29,67). What was not known is whether stimulating MFN activity would have any benefits in conditions, like SOD1 mutant ALS, where the underlying causal lesion is neither an abnormality of MFNs nor a primary imbalance between mitochondrial fusion and fission. The current results show that enhancing mitochondrial dynamics (i.e. fusion and motility) can have salutary effects in at least one condition wherein mitochondrial damage is a secondary contributor to disease.

MFN activators are a relatively new class of bioactive small molecules that, to our knowledge, are the only compounds to directly stimulate mitochondrial fusion and transport. Several MFN activator chemical backbones have been described (43,44,46,72). All of these chemical MFN activators mimic the allosteric mechanism of action originally described for an MFN2-derived peptide, MP-1, which competes with specific peptide–peptide interactions (PPI) that regulate MFN1 and MFN2

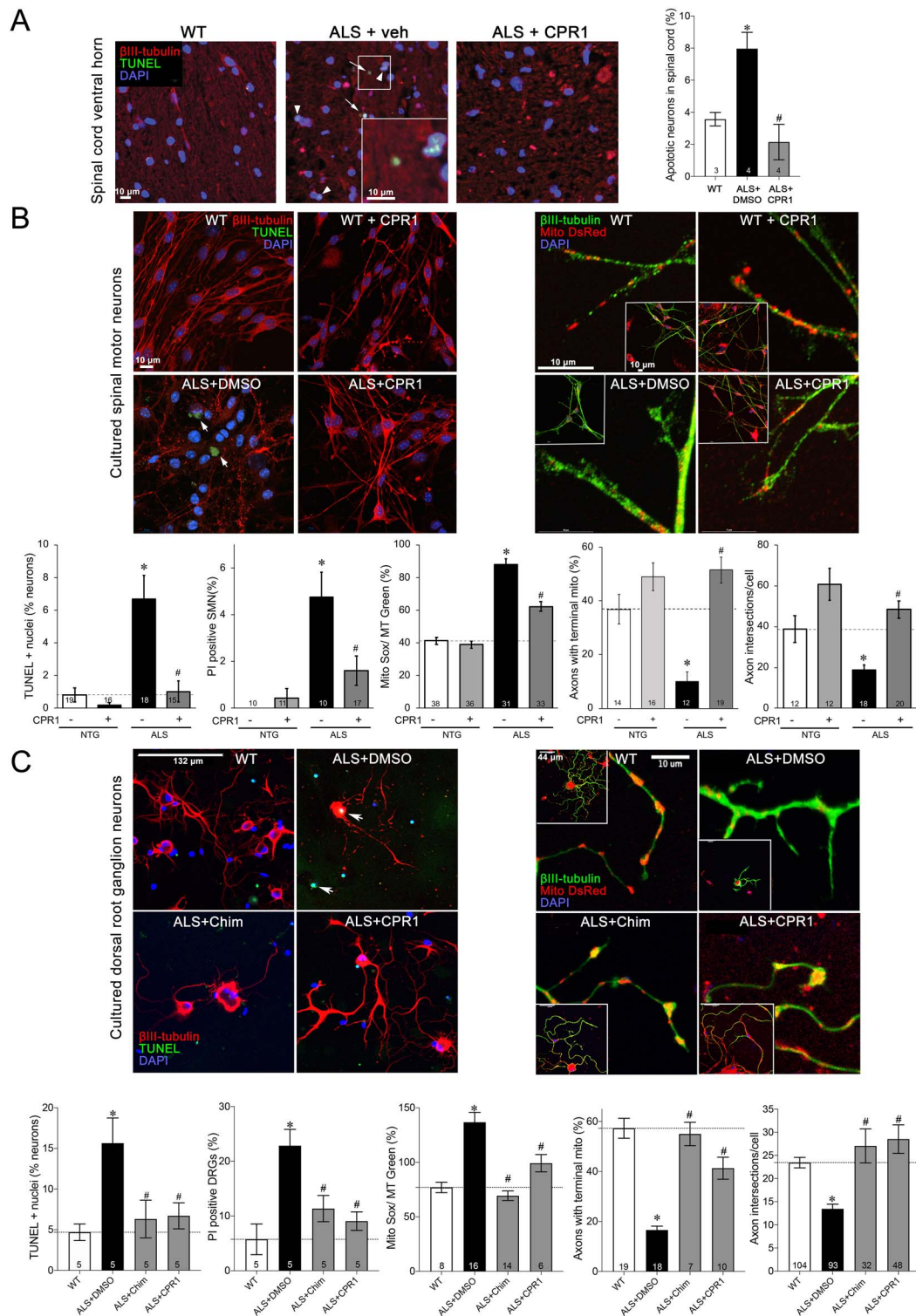


Figure 5. *In vivo* and *in vitro* neuroprotection for SOD1 G93A neurons after mitofusin activation. **(A)** TUNEL (green) staining of apoptotic motor neuron nuclei in lumbar spine ventral horn. Arrows indicate late, and arrow heads early, apoptosis (see inset); quantitative data are to the right. **(B)** Effects of mitofusin activators on programmed death (TUNEL and propidium iodide [PI] labeling), mitochondrial ROS production (Mito-SOX), and neurotrophism (terminal mitochondria and axon branching [intersections]) in cultured spinal motor neurons. Representative TUNEL and branching studies are shown above. **(C)** Parallel studies to (B) of dorsal root sensory neurons. Results are mean \pm SEM; * = $P < 0.05$ vs wild-type (WT/NTG vehicle) normal control; # = $P < 0.05$ vs vehicle-treated ALS (ALS) by ANOVA. Number of mice/cells evaluated per group is indicated at the base of bars in graphs.

conformation (73). Thus, MFN 'zipper domain' (human MFN2 367–384) PPI enforces a folded, more compact MFN conformation unfavorable for mitochondrial fusion and motility (44,73), and interrupting ('unzipping') this PPI with a competing peptide

or small molecule peptidomimetic increases the probability that MFNs will adopt the extended or unfolded conformation favoring mitochondrial fusion and motility. This mechanism of action recently received independent confirmation for compound

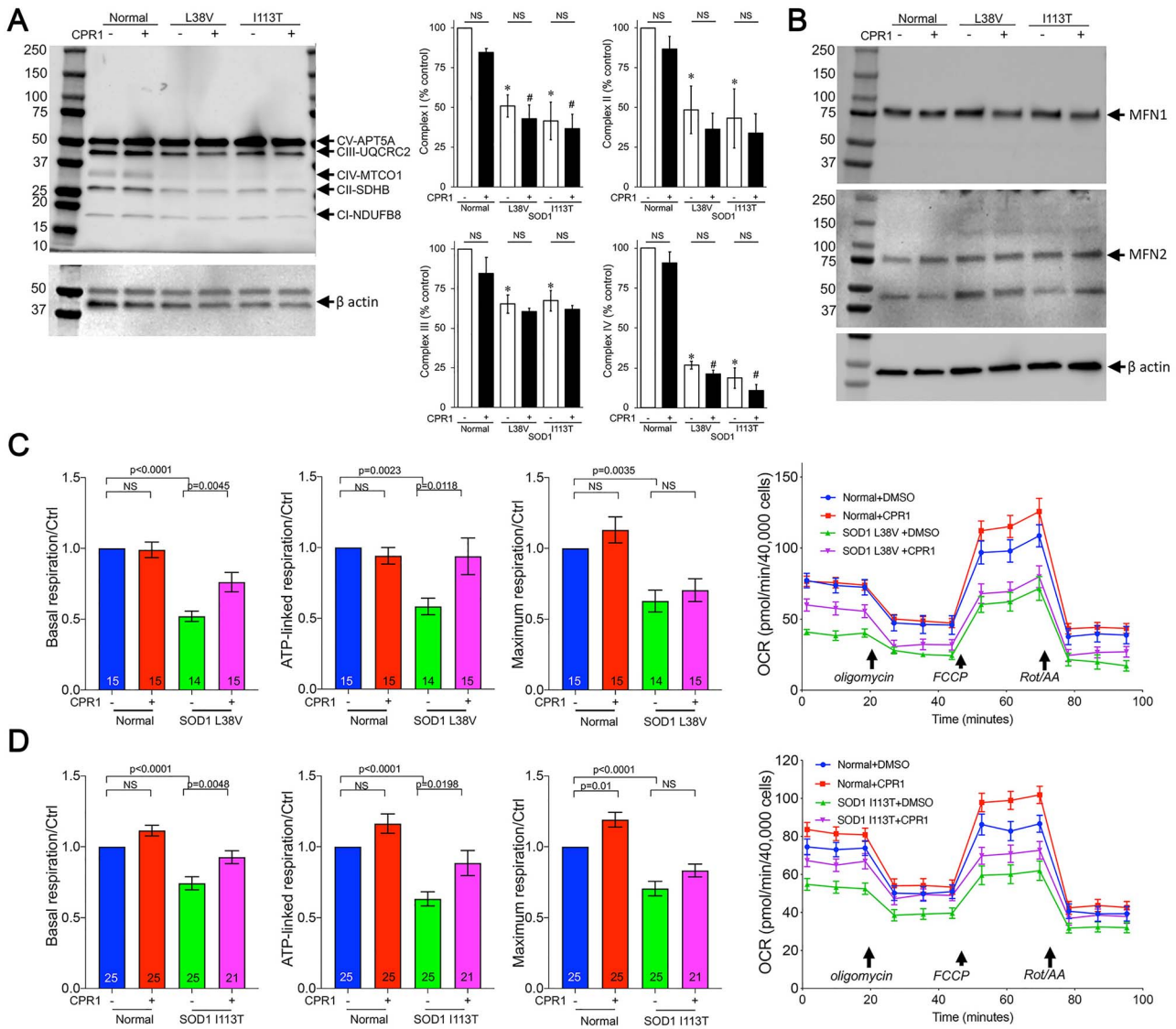


Figure 6. Mitofusin activation improves respiratory coupling in SOD1 mutant reprogrammed ALS motor neurons. **(A)** Immunoblot analysis (representative of 3) of respiratory complex proteins in normal and SOD1 mutant patient reprogrammed motor neurons treated with vehicle or 100 nM CPR1 (48 h). Protein band quantification ($n=3$) is to the right. **(B)** Immunoblot analysis of mitofusin expression in the same samples as **(A)**. **(C, D)** Results of Seahorse oxygen consumption studies in ALS SOD1 L38V **(C)** and SOD1 I113T **(D)** reprogrammed neurons. Group data are to the left (indicated number of samples are individual wells from at 4–5 independent studies). OCR = oxygen consumption rate (pmol/min/40 000 cells). Aggregate data tracings are to the right; Rot/AA = rotenone/antimycin A. Data are mean \pm SEM. P values by ANOVA; NS = non-significant.

‘MASM7’ (74), which was renamed, but is identical to compound ‘B01’ from reference (44), and is one of the parent compounds from which Chimera C was derived. Because MFN ‘unzipping’ mimics the natural process for regulating MFN conformation/activity by phosphorylation of MFN2 S378 (44,75), we speculate that allosteric MFN activation may be better tolerated than perturbing MFN expression or catalytic activity. Indeed, MFN overexpression and activation seemingly have no adverse effects on normal cells or mice (25,29,67).

A major aim of this study was to determine whether activating MFNs could improve mitochondrial phenotypes provoked by ALS-linked SOD1 mutants (6–9). Mitochondrial fragmentation and dysmotility are hallmarks of SOD1 mutant ALS and other neurodegenerative conditions (1), but MFNs are not frequently implicated as causing these abnormalities. Instead, increased mitochondrial fission (21) and a damaged dynein/microtubule mitochondrial

transport system (15) have been proposed, and several other suspect mechanisms are posited to contribute to mitochondrial dysfunction in SOD1 mutant ALS (10,11). Taken together, published data suggest that abnormalities of mitochondrial morphology, transport and respiration are multifactorial. This idea is consistent with the hypothesis that a vicious feedforward cycle exists in which an initial mitochondrial insult provokes ever greater mitochondrial dysfunction, ultimately culminating in neuronal damage and demise (1,11). In this context, general measures (like MFN activation) that can enhance mitochondrial resistance to, and recovery from, diverse forms of injury might have therapeutic value in combination with targeting the underlying causal genetic mechanism.

Given that ALS is a disease of motor neurons, it was notable that we observed mitochondrial fragmentation and loss of polarization in SOD1 mutant fibroblasts as well as (motor and

sensory) neurons. On one hand, this is consistent with SOD1 mutations being germ-line genetic abnormalities affecting multiple cell types. On the other hand, this seems inconsistent with motor neuron selectivity of neuronal pathology. We surmise that motor neuron selectivity in SOD1 mutant ALS is largely driven by non-mitochondrial factors. However, the observation that mitochondrial abnormalities are widespread indicates that systemic therapy, rather than therapies specifically targeted to the central and peripheral nervous systems, could have improved therapeutic benefits.

Our results identify a number of benefits of MFN activation in SOD1 mutant ALS. Not only were mitochondrial fragmentation, hypopolarization and dysmotility in SOD1 mutant cells improved (likely as a direct consequence of increased MFN activity), but the characteristic impairment of mitochondrial ATP-linked respiration in this condition was improved and the hallmark increase in mitochondrial ROS production was suppressed. It is not surprising that these mitochondrial respiration and ROS production were linked as they are reciprocally regulated *in situ*: normal coupling of mitochondrial oxidative phosphorylation to ATP production minimizes mitochondrial ROS elaboration, whereas uncoupling of the electron transport chain from ATP synthesis increases mitochondrial ROS production (76). The current results cannot unambiguously show that improved mitochondrial respiratory coupling from MFN activation underlies enhanced neuronal survival and functioning in ALS SOD1 mutant mice, but this is at least a reasonable prospect. While it is not clear that MFN activators will ever be approved for use in human subjects, if they are they could constitute one component of combination therapy aimed at delaying neuromuscular degeneration to improve quality of life in SOD1 mutant ALS.

Materials and Methods

Mouse lines

SOD1-Gly93Ala (G93A) transgenic mice (B6SJL-Tg(SOD1*G93A)1Gur//) and C57BL/6 J mice were purchased from The Jackson Laboratory (Bar Harbor, ME, USA; Stock #: 002726, Stock: 000664).

Cultured cells

Directly reprogrammed human motor neurons were generated from human dermal fibroblasts as described (29,45).

Adult mouse DRG neurons were prepared from 8- to 12-week-old C57BL/6 J or SOD1 G93A transgenic mice as described (29).

Embryonic mSMN were prepared from E14.5 SOD1 G93A transgenic or non-transgenic littermates according to a published protocol (77). Briefly, individual spinal cords were dissected into four pieces in 1 ml papain solution (2 mg/ml in HBSS, Sigma Cat#: P4762) in wells of 24-well plates and incubated at 37°C for 20 min. Papain digestion was quenched by adding 3 ml cold L-15 medium (Gibco Cat#: 11415-064). The reactants were transferred into 15 ml tubes, gently triturated tissues using a 10 ml suction pipette and the cells pelleted by centrifugation at 280 x g for 10 min at 4°C. Motor neurons were recovered after resuspension in ice cold L-15 medium by application to the surface of Nycodenz solution (1.06 g/ml, Genprice Cat#: 18003) and centrifugation at 900 g for 20 min at 4°C; the interface containing motor neurons was transferred to 50 ml tubes, diluted with L-15 medium up to 50 ml, and centrifuged at 425 g for 10 min at 4°C (to remove the remaining Nycodenz solution). Motor neurons from each spinal cord were resuspended in 2 ml motor neuron medium [1:1 ratio DH medium (DME-Ham 3:1 medium supplemented with NaHCO₃ 36.54 mM, L-adenine 0.18 mM, 2 N HCL 312.5 μL/L, 10% FBS) and neurobasal

A medium (Gibco Cat#: 21103-049), supplemented with 1% B-27 (Gibco Cat#:17504-044), 0.24 mM L-glutamine (Gibco Cat#: 25030-149), 0.2 μg/ml hydrocortisone (Calbiochem Cat#: 386698), 2.5 μg/ml insulin (Sigma Cat#: 11882), 10 ng/ml NT3 (Peprotech Cat# 450-03), 10 ng/ml GDNF (Peprotech Cat# 450-10), 10 ng/ml BDNF (Peprotech Cat# 450-02) and 10 ng/ml CNTF (Peprotech Cat# 450-13)], and plated (400 000/single 12 plate well) on poly-D-lysine (0.1 mg/ml, Sigma Cat#: P7886) coated 18 mm coverslips. Genotypes were determined by assaying the parent embryos and motor neuron lineage was determined by co-staining with β-III tubulin and HB-9 (see Fig. 4A). mSMNs were treated with DMSO or CPR1 (100 nM, 48 h) at day 14 for mitochondrial aspect ratio, depolarization, ROS production and motility analysis. Treatments were started at day 5 for axon branching Sholl analysis and terminal mitochondria occupancy analysis.

SOD1G93A transgenic or non-transgenic MEFs were prepared by enzymatic dissociation from same embryonic day E.14.5 mice used for spinal motor neuron isolation.

PCR genotyping of mutations in ALS and Frontotemporal Dementia (FTD) patient fibroblasts

DNA was extracted from 5 × 10⁶ primary human fibroblasts using the DNeasy blood & tissue kit (Qiagen, Cat#: 69506) according to manufacturer's protocol. PCR of SOD1, TDP43 and FUS gene fragments of interest was performed (initial denaturation at 95°C for 5 min, followed by 30 cycles of denaturation: 95°C, 30 s, annealing: 55°C 30 s, extension: 72°C, 30 s), final extension at 68°C for 5 min, then hold at 4°C) using Taq Plus Master Mix 2X (Cat#: BETAQR-L, Bulls eye), 50 ng of genomic DNA template, and the following primers:

ALS:

SOD1 L38V-fw 5'-CTTCACTGTGAGGGGTAAGG-3'
 SOD1 L38V-rv 5'-CTAGGGTGAACAAGTATGGG-3'
 SOD1 I113T-fw 5'-TGTTTGTAGTGGCATCAGCCCT-3'
 SOD1 I113T-rv 5'-ACCGCGACTAACAATCAAAGTG-3'
 SOD1 L145F-fw 5'-GGTAGTGATTACTTGACAGCCCAA-3'
 SOD1 L145F-rv 5'-GTAAAGGGGCTCAGACTACAT-3'
 TDP43 A382T-fw 5'-AACATGCAGAGGGAGCCAAA-3'
 TDP43 A382T-rv 5'-ACCCTGCATTGGATGCTGAT-3'
 FUS R521G-fw 5'-TACTCGCTGGGTTAGGTAGGA-3'
 FUS R521G-rv 5'-ACGAGGGTAACACTGGGTACA-3'

PCR products were purified using PureLink Quick Gel Extraction Kit (Invitrogen, Cat#: K2100-12) and sent to GENEWIZ for Sanger sequencing.

Imaging

Static confocal imaging of live cultured neurons used triple staining with MitoTracker Green (200 nM, 30 min; Invitrogen, Thermo Fisher Scientific Cat#: M7514) to visualize mitochondria, tetramethylrhodamine ethyl ester (TMRE, 200 nM, 30 min; Invitrogen Thermo Fisher Scientific Cat#: T-669) or MitoSOX Red (5 μM, 10 min; Invitrogen Thermo Fisher Scientific Cat#: M36008) and Hoechst (10 μg/ml, 30 min; Invitrogen, Thermo Fisher Scientific Cat#: H3570) that stains nuclei blue. Static live cell images were acquired on a Nikon Ti Confocal microscope using either a 60X1.3 NA oil-immersion objective, in Krebs-Henseleit buffer (138 mM NaCl, 3.7 mM KCl, 1.2 mM KH₂PO₄, 15 mM glucose, 20 mM HEPES pH: 7.2-7.5 and 1 mM CaCl₂). Laser excitation was 488 nm with emission at 510 nm for MitoTracker Green, 488 nm with emission at 590 nm for MitoSOX, 549 nm with emission at 590 nm for TMRE, and 306 nm with emission 405 nm for Hoechst.

Axon branching analysis of mouse DRGs was assessed 48 h after isolation, plating and treatment; 24 h after plating medium was exchanged and drugs re-added. Cells were formalin fixed and labeled with anti- β -tubulin III (mouse monoclonal, 1:200 in 10% goat serum in room temperature PBS for 30 min, BioLegend, Cat#: 801201) and Alexa-Fluor 488 (goat anti-mouse, 1:400 in 10% goat serum in 1XDPBS, ThermoFisher, Cat#: A11029) to identify neurons. Images were acquired using the 10x dry objective and excitation at 488 nm/emission 510 nm for Alexa-Fluor 488 and 579 excitation/599 emission for mito-DSRed. Sholl analysis of axonal branching used ImageJ and an open source plugin (https://imagej.net/Sholl_Analysis) as previously described (29).

Video confocal studies of mitochondrial motility studies in cultured reprogrammed human motor neurons, mouse DRG neurons or mouse sciatic nerve axons used time-lapse imaging (1 frame every 5 s) for 180 frames (15 min) at 37°C on a Nikon A1Rsi Confocal Microscope using a 40 \times oil objective as described (29,44). Kymographs and quantitative data were generated using an Image-J plug-in (Velocity_Measurement_Tool).

In vivo studies in ALS mice (SOD1G93A)

Experimental design—60-day-old male and female SOD1 G93A ALS mice were randomized to treatment with MiM111 (30 mg/kg IM once daily) or vehicle (MiM111 study) or to CPR1 (60 mg/kg PO twice daily) or the same vehicle (10% Me₂SO/90% (30% 2-hydroxypropyl)- β -cyclodextrin [HP- β -CD; Sigma, Cat#:332607]) (CPR1 study). Drugs and vehicle were sterile-filtered (0.22 μ m PVDF, #SLGV033RS, Millipore, Cork, Ireland) and syringes prepared and assigned to mice by LZ according to a randomization table. Drugs were administered to mice by XD who was blind to mouse genotype and treatment group. There were no drug-related adverse effects. Behavioral and neurophysiological testing were performed before and every 10 days after initiation of therapy:

RotaRod testing was performed using a RotaRod from Ugo Basile (Gemonio, Italy; #47650). After initial training at a constant speed of 5 RPM, studies were performed with acceleration from 5 to 40 RPM over 120 s, maintaining 40 RPM thereafter. Mice were tested five times and the average latency time (when the mouse fell from the device) was reported.

Inverted grip testing placed mice in the center of a tight woven mesh in an oval metal frame, which was inverted over 2 s and maintained 40–50 cm above the bottom of cage until the mice fell (latency time). Studies were repeated three times and the average latency time was reported.

A combined neuromuscular dysfunction score used the system described by Guyenet *et al.* (47): **Ledge test**: Score 0 (normal) = effectively use hind legs while walking along the ledge of the cage; Score 1 = loses footing some times while walking along the ledge, but appears coordinated; Score 2 = does not effectively use hind legs; Score 3 = refuses to move along the ledge or falls off while walking; **Hindlimb clasping**: Score 0 (normal) = hindlimbs completely splayed outward while being lifted by its tail; Score 1 = one hindlimb partially collapsed toward the abdomen; Score 2 = both hindlimbs partially collapsed toward the abdomen; Score 3 = hindlimbs entirely touching the abdomen; **Gait**: Score 0 = normal gait; Score 1 = tremor or limp; Score 2 = feet point away from the body while walking; Score 3 = difficulty moving forward; **Kyphosis**: Score 0 (normal) = able to straighten spine while walking, no kyphosis; Score 1 = mild kyphosis but able to straighten spine; Score 2 = unable to straighten spine with mild kyphosis; Score 3 = severe kyphosis while walking and sitting. The results of each test were added together to obtain the combined neuromuscular dysfunction score.

Neuroelectrophysiologic recordings of tibialis/gastrocnemius CMAP. Mice were anesthetized with isoflurane and shaved, and a needle electrode was inserted to stimulate the proximal sciatic nerves (3.9 mV pulses; 0.002 ms duration). Ring electrodes were positioned at the mid forelimb to record CMAP with a Viasys Healthcare Nicolet Biomedical instrument (Middleton, WI, USA Cat#: OL060954) using Viking Quest version 11.2 software. Optimal stimulating electrode position was defined as that giving the greatest CMAP amplitude; three to four independent events were recorded and averaged.

Survival studies. Mice were observed until the level of neuromuscular dysfunction achieved the predetermined endpoint of being unable to right within 30 s of being placed on their backs.

Non-survival endpoint studies were terminated after final testing at the pre-determined age of 140 days. In the 140-day studies sciatic and mid tibial nerves, gastrocnemius muscles and lumbar spinal cord samples were harvested and either frozen in optimal cutting temperature (OCT, Tissue-TEK Cat: 4583) or fixed in 4% PFA/PBS for 2 h, transferred to 30% sucrose/PBS overnight at 4°C and embedded in paraffin. Nerve sections were stained with toluidine blue or immunolabeled with 4-HNE (1:200 in 10% goat serum, r.t., 0.5 h, Abcam Cat#: ab46545) and β -tubulin III (1:200 in 10% goat serum, r.t., 0.5 h, Biolegend Cat#: 801201). Gastrocnemius muscle sections were labeled with fluorescein-conjugated wheat germ agglutinin (Cat#: W834, Invitrogen) to label myocyte membranes and 4-HNE to label ROS for 30 min at room temperature.

NMJs staining used 10 μ m thick frozen sections of gastrocnemius muscle as described (29). Briefly, frozen sections were fixed in precooled (–20°C for 10 min at r.t., blocked with 10% goat serum for 15 min and stained with anti-COX IV (1:200 in 10% goat serum, 4°C, overnight, Cat#: ab16056, Abcam) and labeled neuronal synapses with α -Bungarotoxin (0.5 μ g/ml in 10% goat serum, r.t., 1 h, Cat#: B-13423, Thermo Fisher Scientific).

COX/SDH double staining on 10 μ m frozen gastrocnemius muscle sections used VitroView™ COX-SDH Double Histochemistry Stain Kit (Cat#: VB-3022, VitroVivo Biotech) according to the manufacturer's protocol.

Transmission electron microscopy and toluidine blue staining used standard techniques.

TUNEL staining on mice spinal cords used the DeadEnd Fluorometric TUNEL system (Cat#: G3250, Promega) according to the manufacturer's instructions. Briefly, lumbar spinal cords were fixed in 4%PFA overnight and embedded in paraffin before sectioning. After undergoing deparaffinization, slides were immersed in 0.1% TritonX-100 for 15 min, washed twice with PBS, transferred to 100 μ L equilibration buffer for 10 min, and then reacted with 50 μ L TdT reaction mix for 60 min at 37°C. The reaction was stopped with 2XSSC for 15 min, followed by washing thrice with PBS. Anti- β -tubulin III staining was used to label neurons.

Mitochondrial respiration in reprogrammed ALS motor neurons was measured as the oxygen consumption rate (OCR) using a Seahorse XFe24 Extracellular Flux Analyzer (Seahorse Bioscience, Billerica, MA, USA). Briefly, neurons were plated on the Seahorse XF24-well cell culture microplate (Cat#: 100777-004, Agilent), treated with Chimera or CPR1 (100 nM) or DMSO vehicle and mitochondrial OCR measured 48 h later. Before assays, sensor cartridges (Cat#: 102340-100, Agilent) were hydrated with XF calibrant (1 ml/well, Cat#: 100840-000, Agilent) in a non-CO₂ 37°C incubator overnight. Neurons were washed two times in Seahorse XF assay DMEM medium (Cat#: 103680-100, Agilent) supplemented with 1 mM pyruvate (Cat#: 103578-100, Agilent), 2 mM glutamine (Cat#: 103579-100, Agilent) and 10 mM glucose (Cat#: 103577-100, Agilent); 500 μ L assay medium was added

after final wash, and the cells incubated in a non-CO₂ 37°C incubator for 1 h. After four basal respiration measurements, 1 μ M oligomycin (inhibitor of ATP synthase), 1 μ M FCCP (an optimized concentration to give maximum respiratory capacity) and 0.5 μ M rotenone/antimycin A (Seahorse XF Cell Mito Stress Test Assay, Cat#: 103010-100, Aligent) were autoinjected into the experimental wells. ATP-linked respiration is the decrease in oxygen consumption rate from basal respiration after injection of the ATP synthesis inhibitor oligomycin, data reported as basal OCR-post oligomycin OCR for each well. Each experimental column is an average of a minimum of five replicate wells and each experiment was performed with a minimum of three biological replicates.

CPR1 toxicity was assessed in 12-week-old female C57BL6/J mice (The Jackson Laboratory, Bar Harbor, ME, USA, Stock #: 000664) that received 60 mg/kg CPR1 in 10% DMSO/90% (30% HP- β -CD) or vehicle alone twice daily for 28 days via oral gavage. Cage-side clinical observations were made daily. At study termination on day 28 mice were sacrificed with an overdose of isoflurane followed by cervical dislocation and blood collected via left ventricular puncture. Blood hematology and chemical analyses were performed by Washington University, Division of Comparative Medicine Research Animal Diagnostic Laboratory (St. Louis, MO, USA).

Antioxidant capacity assays used total antioxidant capacity assay kit (Cellbiolabs, Cat#: STA360), catalase activity assay kit (Cellbiolabs, Cat#: STA341) and superoxide dismutase activity assay (Cellbiolabs, Cat#: STA341) according to the manufacturer's protocols. CPR1 (1 μ M) or DMSO was added to standard concentrations of uric acid, superoxide dismutase or catalase standard within a 96-well microtiter plate format. Samples and standards were diluted with the proper reaction reagent and, upon the addition of copper, hydrogen peroxide or xanthine solution/xanthine oxidase solution, reacted for 5 min or 1 h as per manufacturer's instructions. The reactants were stopped and assayed using a 96-well spectrophotometric microplate reader at 490 or 520 nm.

Misfolded SOD1 aggregation analysis was assayed in 140 days mice brains by using immunoblot analysis. Briefly, mice brains were homogenized with ultra turrax homogenizer set at level 6 for 30 K RPM for 1 min, in tissue extraction buffer (Invitrogen Cat#: FNN0071), added 1 mM phenylmethylsulfonyl fluoride (PMSF), protease inhibitor (Roche Cat#: 05892970001) and phosphatase inhibitor (Roche Cat#: 04906837001). Homogenates were spin down at 200 g for 10 min at 4°C, 1000 g for 10 min at 4°C and 3800 g for 10 min at 4°C, then 17000 g for 15 min at 4°C, transfer supernatants (post-mitochondria) to a new tube, resuspend mitochondria pellet in tissue extraction buffer. Approximately 40 μ g protein were loaded and run on 4–20% pre-cast SDS-PAGE gels (Bio-Rad Cat#: 4561096) with constant voltage (90 mV), and transferred to polyvinylidene fluoride (PVDF) membranes (GE Healthcare, 10600021) at 4°C using 110 mV for an hour in transfer buffer containing 20% methanol. After blocked in 5% non-fat milk (Bio-Rad Cat#: 1706404) for 30 min at room temperature, membranes were incubated with primary antibodies (Anti-SOD1, 1:1000, Abcam Cat#: ab51254; Anti-misfolded SOD1, 1:400, MEDIMABS Cat#: MM-0070-2-P; Anti-COX IV, 1:1000, Abcam Cat#: ab16056; Anti- β actin, 1:2000, Proteintech Cat#: 66009-1-Ig) diluted in blocking buffer overnight at 4°C, followed by incubation with secondary antibodies (Anti-mouse IgG, 1:2000, Cell Signaling Technology Cat#: cs7076; Anti-rabbit IgG, 1:2000, Cell Signaling Technology Cat#: cs7074) diluted in blocking buffer at room temperature for 1 h. Immunoblot signals were detected by using LI-COR Odyssey imaging system. Immunoblot membranes were

stripped by using western blot stripping buffer (Thermo Fisher Cat#: 46430) according to the manufacturer's instruction before re-probed.

Statistics

Unless otherwise stated, data are reported as means \pm SEM. Two-group comparisons used Student's t-test; multiple group comparisons used one-way ANOVA; time course by treatment group or genotype by treatment group comparisons used two-way ANOVA with Tukey's post-hoc test for individual statistical comparisons. $P < 0.05$ was considered significant. The details of statistical methods, exact values of n and what n represents are indicated in figures and figure legends.

Mouse treatment was randomized according to a random integer table (even or odd) and performed by investigators blind to treatment status. Post-terminal analysis of tissues was performed blindly.

Study approval

All experimental procedures were approved by Washington University in St. Louis School of Medicine Animal Studies Committee; IACUC protocol number 19-0910, Exp:12/16/2022.

Supplementary Material

Supplementary Material is available at HMG online.

Acknowledgements

G.W.D. is the Philip and Sima K. Needleman-endowed Professor at Washington University in St. Louis and a past Scholar-Innovator awardee of the Harrington Discovery Institute. The authors are grateful for helpful discussions with Professor Daria Mochly-Rosen of Stanford University.

Funding

This work was supported by the National Institutes of Health (R42NS113642, R42NS115184 and R35HL135736 to G.W.D.); the China Scholarship Council (to X.D.) and the Muscular Dystrophy Association (Research Grant 628906 to G.W.D.).

Competing Interests

G.W.D. is an inventor on multiple patents owned by Washington University and other entities that cover the use of small molecule mitofusin activators to treat neurodegenerative diseases. G.W.D. is the founder of Mitochondria in Motion, Inc., a Saint Louis based biotech R&D company that aims to enhance mitochondrial trafficking and fitness in neurodegenerative diseases. The other authors declare no competing interests. Studies with MiM111 and CPR1 were performed under terms of an MTA between Mitochondria in Motion, Inc. and Washington University in St. Louis.

Authors' Contributions

G.W.D. conceived of and designed the research. G.W.D. and X.D. wrote the manuscript. X.D. and L.Z. performed all mouse studies. A.F. and X.D. performed ALS DRG experiments. X.D. performed all *in vitro* and *ex vivo* mitochondrial studies.

References

- Knott, A.B., Perkins, G., Schwarzenbacher, R. and Bossy-Wetzel, E. (2008) Mitochondrial fragmentation in neurodegeneration. *Nat. Rev. Neurosci.*, **9**, 505–518.
- Burte, F., Carelli, V., Chinnery, P.F. and Yu-Wai-Man, P. (2015) Disturbed mitochondrial dynamics and neurodegenerative disorders. *Nat. Rev. Neurol.*, **11**, 11–24.
- Monzio Compagnoni, G., Di Fonzo, A., Corti, S., Comi, G.P., Bresolin, N. and Masliah, E. (2020) The role of mitochondria in neurodegenerative diseases, the lesson from Alzheimer's disease and Parkinson's disease. *Mol. Neurobiol.*, **57**, 2950–2980.
- Rosen, D.R., Siddique, T., Patterson, D., Figlewicz, D.A., Sapp, P., Hentati, A., Donaldson, D., Goto, J., O'Regan, J.P., Deng, H.X. et al. (1993) Mutations in Cu/Zn superoxide dismutase gene are associated with familial amyotrophic lateral sclerosis. *Nature*, **362**, 59–62.
- Deng, H.X., Hentati, A., Tainer, J.A., Iqbal, Z., Cayabyab, A., Hung, W.Y., Getzoff, E.D., Hu, P., Herzfeldt, B., Roos, R.P. et al. (1993) Amyotrophic lateral sclerosis and structural defects in Cu,Zn superoxide dismutase. *Science*, **261**, 1047–1051.
- Kong, J. and Xu, Z. (1998) Massive mitochondrial degeneration in motor neurons triggers the onset of amyotrophic lateral sclerosis in mice expressing a mutant SOD1. *J. Neurosci.*, **18**, 3241–3250.
- Mattiazzi, M., D'Aurelio, M., Gajewski, C.D., Martushova, K., Kiaei, M., Beal, M.F. and Manfredi, G. (2002) Mutated human SOD1 causes dysfunction of oxidative phosphorylation in mitochondria of transgenic mice. *J. Biol. Chem.*, **277**, 29626–29633.
- De Vos, K.J., Chapman, A.L., Tennant, M.E., Manser, C., Tudor, E.L., Lau, K.F., Brownlee, J., Ackerley, S., Shaw, P.J., McLoughlin, D.M. et al. (2007) Familial amyotrophic lateral sclerosis-linked SOD1 mutants perturb fast axonal transport to reduce axonal mitochondria content. *Hum. Mol. Genet.*, **16**, 2720–2728.
- Magrané, J., Cortez, C., Gan, W.B. and Manfredi, G. (2014) Abnormal mitochondrial transport and morphology are common pathological denominators in SOD1 and TDP43 ALS mouse models. *Hum. Mol. Genet.*, **23**, 1413–1424.
- Tafari, F., Ronchi, D., Magri, F., Comi, G.P. and Corti, S. (2015) SOD1 misplacing and mitochondrial dysfunction in amyotrophic lateral sclerosis pathogenesis. *Front. Cell. Neurosci.*, **9**, 336.
- Smith, E.F., Shaw, P.J. and De Vos, K.J. (2019) The role of mitochondria in amyotrophic lateral sclerosis. *Neurosci. Lett.*, **710**, 132933.
- Jaarsma, D., Rognoni, F., van Duijn, W., Verspaget, H.W., Haasdijk, E.D. and Holstege, J.C. (2001) CuZn superoxide dismutase (SOD1) accumulates in vacuolated mitochondria in transgenic mice expressing amyotrophic lateral sclerosis-linked SOD1 mutations. *Acta Neuropathol.*, **102**, 293–305.
- Liu, J., Lillo, C., Jonsson, P.A., Vande Velde, C., Ward, C.M., Miller, T.M., Subramaniam, J.R., Rothstein, J.D., Marklund, S., Andersen, P.M. et al. (2004) Toxicity of familial ALS-linked SOD1 mutants from selective recruitment to spinal mitochondria. *Neuron*, **43**, 5–17.
- Culik, R.M., Sekhar, A., Nagesh, J., Deol, H., Rumpf, J.A.O., Meiering, E.M. and Kay, L.E. (2018) Effects of maturation on the conformational free-energy landscape of SOD1. *Proc. Natl. Acad. Sci. U. S. A.*, **115**, E2546–E2555.
- Ligon, L.A., LaMonte, B.H., Wallace, K.E., Weber, N., Kalb, R.G. and Holzbaur, E.L. (2005) Mutant superoxide dismutase disrupts cytoplasmic dynein in motor neurons. *Neuroreport*, **16**, 533–536.
- Tan, W., Pasinelli, P. and Trotti, D. (2014) Role of mitochondria in mutant SOD1 linked amyotrophic lateral sclerosis. *Biochim. Biophys. Acta*, **1842**, 1295–1301.
- Zhang, S., Zhao, J., Quan, Z., Li, H. and Qing, H. (2022) Mitochondria and other organelles in neural development and their potential as therapeutic targets in neurodegenerative diseases. *Front. Neurosci.*, **16**, 853911.
- Szeto, H.H. (2014) First-in-class cardiolipin-protective compound as a therapeutic agent to restore mitochondrial bioenergetics. *Br. J. Pharmacol.*, **171**, 2029–2050.
- Qi, X., Qvit, N., Su, Y.C. and Mochly-Rosen, D. (2013) A novel Drp1 inhibitor diminishes aberrant mitochondrial fission and neurotoxicity. *J. Cell Sci.*, **126**, 789–802.
- Petri, S., Kiaei, M., Damiano, M., Hiller, A., Wille, E., Manfredi, G., Calingasan, N.Y., Szeto, H.H. and Beal, M.F. (2006) Cell-permeable peptide antioxidants as a novel therapeutic approach in a mouse model of amyotrophic lateral sclerosis. *J. Neurochem.*, **98**, 1141–1148.
- Joshi, A.U., Saw, N.L., Vogel, H., Cunningham, A.D., Shamloo, M. and Mochly-Rosen, D. (2018) Inhibition of Drp1/Fis1 interaction slows progression of amyotrophic lateral sclerosis. *EMBO Mol. Med.*, **10**, e8166.
- Chan, D.C. (2020) Mitochondrial dynamics and its involvement in disease. *Annu. Rev. Pathol.*, **15**, 235–259.
- Santel, A. and Fuller, M.T. (2001) Control of mitochondrial morphology by a human mitofusin. *J. Cell Sci.*, **114**, 867–874.
- Dorn, G.W., 2nd (2019) Evolving concepts of mitochondrial dynamics. *Annu. Rev. Physiol.*, **81**, 1–17.
- Detmer, S.A. and Chan, D.C. (2007) Complementation between mouse Mfn1 and Mfn2 protects mitochondrial fusion defects caused by CMT2A disease mutations. *J. Cell Biol.*, **176**, 405–414.
- Dang, X., Walton, E.K., Zablocka, B., Baloh, R.H., Shy, M.E., Dorn, G.W. and 2nd. (2022) Mitochondrial phenotypes in genetically diverse neurodegenerative diseases and their response to mitofusin activation. *Cell*, **11**, 1053.
- Baloh, R.H., Schmidt, R.E., Pestronk, A. and Milbrandt, J. (2007) Altered axonal mitochondrial transport in the pathogenesis of Charcot-Marie-Tooth disease from mitofusin 2 mutations. *J. Neurosci.*, **27**, 422–430.
- Bernard-Marissal, N., van Hameren, G., Juneja, M., Pellegrino, C., Louhivuori, L., Bartesaghi, L., Rochat, C., El Mansour, O., Médard, J.J., Croisier, M. et al. (2019) Altered interplay between endoplasmic reticulum and mitochondria in Charcot-Marie-Tooth type 2A neuropathy. *Proc. Natl. Acad. Sci. U. S. A.*, **116**, 2328–2337.
- Franco, A., Dang, X., Walton, E.K., Ho, J.N., Zablocka, B., Ly, C., Miller, T.M., Baloh, R.H., Shy, M.E., Yoo, A.S. et al. (2020) Burst mitofusin activation reverses neuromuscular dysfunction in murine CMT2A. *elife*, **9**, e61119.
- Schiavon, C.R., Shadel, G.S. and Manor, U. (2021) Impaired mitochondrial mobility in Charcot-Marie-Tooth disease. *Front. Cell Dev. Biol.*, **9**, 624823.
- Baloh, R.H. (2008) Mitochondrial dynamics and peripheral neuropathy. *Neuroscientist*, **14**, 12–18.
- Misko, A., Jiang, S., Wegorzewska, I., Milbrandt, J. and Baloh, R.H. (2010) Mitofusin 2 is necessary for transport of axonal mitochondria and interacts with the Miro/Milton complex. *J. Neurosci.*, **30**, 4232–4240.
- Naon, D. and Scorrano, L. (2014) At the right distance, ER-mitochondria juxtaposition in cell life and death. *Biochim. Biophys. Acta*, **1843**, 2184–2194.
- Janikiewicz, J., Szymański, J., Malinska, D., Patalas-Krawczyk, P., Michalska, B., Duszyński, J., Giorgi, C., Bonora, M., Dobrzyn, A. and Wieckowski, M.R. (2018) Mitochondria-associated membranes in aging and senescence, structure, function, and dynamics. *Cell Death Dis.*, **9**, 332.

35. Emery, J.M. and Ortiz, R.M. (2021) Mitofusin 2, A link between mitochondrial function and substrate metabolism? *Mitochondrion*, **61**, 125–137.
36. Gurney, M.E., Pu, H., Chiu, A.Y., Dal Canto, M.C., Polchow, C.Y., Alexander, D.D., Caliendo, J., Hentati, A., Kwon, Y.W., Deng, H.X. et al. (1994) Motor neuron degeneration in mice that express a human Cu,Zn superoxide dismutase mutation. *Science*, **264**, 1772–1775.
37. Martin, L.J. (2007) Transgenic mice with human mutant genes causing Parkinson's disease and amyotrophic lateral sclerosis provide common insight into mechanisms of motor neuron selective vulnerability to degeneration. *Rev. Neurosci.*, **18**, 115–136.
38. Beresewicz, M., Boratynska-Jasinska, A., Charzewski, L., Kawalec, M., Kabzinska, D., Kochanski, A., Krzysko, K.A. and Zablocka, B. (2017) The effect of a novel c.820C>T (Arg274Trp) mutation in the mitofusin 2 gene on fibroblast metabolism and clinical manifestation in a patient. *PLoS One*, **12**, e0169999.
39. Aguer, C., Gambarotta, D., Mailloux, R.J., Moffat, C., Dent, R., McPherson, R. and Harper, M.E. (2011) Galactose enhances oxidative metabolism and reveals mitochondrial dysfunction in human primary muscle cells. *PLoS One*, **6**, e28536.
40. Dorn, G.W., 2nd and Dang, X. (2022) Predicting mitochondrial dynamic behavior in genetically defined neurodegenerative diseases. *Cell*, **111**, 1046.
41. van der Blik, A.M., Shen, Q. and Kawajiri, S. (2013) Mechanisms of mitochondrial fission and fusion. *Cold Spring Harb. Perspect. Biol.*, **5**, a011072.
42. Crowley, L.C., Christensen, M.E. and Waterhouse, N.J. (2016) Measuring mitochondrial transmembrane potential by TMRE staining. *Cold Spring Harb. Protoc.*, **2016**, pdb.prot087361.
43. Dang, X., Zhang, L., Franco, A., Li, J., Rocha, A.G., Devanathan, S., Dolle, R.E., Bernstein, P.R. and Dorn, G.W., 2nd (2020) Discovery of 6-phenylhexanamide derivatives as potent stereoselective mitofusin activators for the treatment of mitochondrial diseases. *J. Med. Chem.*, **63**, 7033–7051.
44. Rocha, A.G., Franco, A., Krezel, A.M., Rumsey, J.M., Alberti, J.M., Knight, W.C., Biris, N., Zacharioudakis, E., Janetka, J.W., Baloh, R.H. et al. (2018) MFN2 agonists reverse mitochondrial defects in preclinical models of Charcot-Marie-Tooth disease type 2A. *Science*, **360**, 336–341.
45. Abernathy, D.G., Kim, W.K., McCoy, M.J., Lake, A.M., Ouwenga, R., Lee, S.W., Xing, X., Li, D., Lee, H.J., Heuckeroth, R.O. et al. (2017) MicroRNAs induce a permissive chromatin environment that enables neuronal subtype-specific reprogramming of adult human fibroblasts. *Cell Stem Cell*, **21**, 332–348.e339.
46. Dang, X., Williams, S.B., Devanathan, S., Franco, A., Fu, L., Bernstein, P.R., Walters, D., Dorn, G.W. and 2nd. (2021) Pharmacophore-based design of phenyl-[hydroxycyclohexyl] cycloalkyl-carboxamide mitofusin activators with improved neuronal activity. *J. Med. Chem.*, **64**, 12506–12524.
47. Guyenet, S.J., Furrer, S.A., Damian, V.M., Baughan, T.D., La Spada, A.R. and Garden, G.A. (2010) A simple composite phenotype scoring system for evaluating mouse models of cerebellar ataxia. *J. Vis. Exp.*, **39**, 1787.
48. Daube, J.R. (2000) Electrodiagnostic studies in amyotrophic lateral sclerosis and other motor neuron disorders. *Muscle Nerve*, **23**, 1488–1502.
49. Heiman-Patterson, T.D., Deitch, J.S., Blankenhorn, E.P., Erwin, K.L., Perreault, M.J., Alexander, B.K., Byers, N., Toman, I. and Alexander, G.M. (2005) Background and gender effects on survival in the TgN(SOD1-G93A)1Gur mouse model of ALS. *J. Neurol. Sci.*, **236**, 1–7.
50. Sasaki, S. and Iwata, M. (2007) Mitochondrial alterations in the spinal cord of patients with sporadic amyotrophic lateral sclerosis. *J. Neuropathol. Exp. Neurol.*, **66**, 10–16.
51. Pasinelli, P., Belford, M.E., Lennon, N., Bacskai, B.J., Hyman, B.T., Trotti, D. and Brown, R.H., Jr. (2004) Amyotrophic lateral sclerosis-associated SOD1 mutant proteins bind and aggregate with Bcl-2 in spinal cord mitochondria. *Neuron*, **43**, 19–30.
52. Pedrini, S., Sau, D., Guareschi, S., Bogush, M., Brown, R.H., Jr., Naniche, N., Kia, A., Trotti, D. and Pasinelli, P. (2010) ALS-linked mutant SOD1 damages mitochondria by promoting conformational changes in Bcl-2. *Hum. Mol. Genet.*, **19**, 2974–2986.
53. Lee, J.K., Hwang, S.G., Shin, J.H., Shim, J. and Choi, E.J. (2014) CIIA prevents SOD1(G93A)-induced cytotoxicity by blocking ASK1-mediated signaling. *Front. Cell. Neurosci.*, **8**, 179.
54. Pickles, S., Destroismaisons, L., Peyrard, S.L., Cadot, S., Rouleau, G.A., Brown, R.H., Jr., Julien, J.P., Arbour, N. and Vande Velde, C. (2013) Mitochondrial damage revealed by immunoselection for ALS-linked misfolded SOD1. *Hum. Mol. Genet.*, **22**, 3947–3959.
55. Sakellariou, G.K., Pye, D., Vasilaki, A., Zibrik, L., Palomero, J., Kabayo, T., McArdle, F., Van Remmen, H., Richardson, A., Tidball, J.G. et al. (2011) Role of superoxide-nitric oxide interactions in the accelerated age-related loss of muscle mass in mice lacking Cu,Zn superoxide dismutase. *Aging Cell*, **10**, 749–760.
56. Guégan, C., Vila, M., Rosoklija, G., Hays, A.P. and Przedborski, S. (2001) Recruitment of the mitochondrial-dependent apoptotic pathway in amyotrophic lateral sclerosis. *J. Neurosci.*, **21**, 6569–6576.
57. Kirkinetzos, I.G., Bacman, S.R., Hernandez, D., Oca-Cossio, J., Arias, L.J., Perez-Pinzon, M.A., Bradley, W.G. and Moraes, C.T. (2005) Cytochrome c association with the inner mitochondrial membrane is impaired in the CNS of G93A-SOD1 mice. *J. Neurosci.*, **25**, 164–172.
58. Gu, X., Ma, Y., Liu, Y. and Wan, Q. (2021) Measurement of mitochondrial respiration in adherent cells by Seahorse XF96 Cell Mito Stress Test. *STAR Protoc.*, **2**, 100245.
59. Browne, S.E., Yang, L., DiMauro, J.P., Fuller, S.W., Licata, S.C. and Beal, M.F. (2006) Bioenergetic abnormalities in discrete cerebral motor pathways presage spinal cord pathology in the G93A SOD1 mouse model of ALS. *Neurobiol. Dis.*, **22**, 599–610.
60. Cousse, E., De Smet, P., Bogaert, E., Elens, I., Van Damme, P., Willems, P., Koopman, W., Van Den Bosch, L. and Callewaert, G. (2011) G37R SOD1 mutant alters mitochondrial complex I activity, Ca(2+) uptake and ATP production. *Cell Calcium*, **49**, 217–225.
61. Chen, H., McCaffery, J.M. and Chan, D.C. (2007) Mitochondrial fusion protects against neurodegeneration in the cerebellum. *Cell*, **130**, 548–562.
62. Chen, Y., Liu, Y., Dorn, G.W. and 2nd. (2011) Mitochondrial fusion is essential for organelle function and cardiac homeostasis. *Circ. Res.*, **109**, 1327–1331.
63. Eschenbacher, W.H., Song, M., Chen, Y., Bhandari, P., Zhao, P., Jowdy, C.C., Engelhard, J.T., Dorn, G.W. and 2nd. (2012) Two rare human mitofusin 2 mutations alter mitochondrial dynamics and induce retinal and cardiac pathology in *Drosophila*. *PLoS One*, **7**, e44296.
64. Kasahara, A., Cipolat, S., Chen, Y., Dorn, G.W., 2nd and Scorrano, L. (2013) Mitochondrial fusion directs cardiomyocyte differentiation via calcineurin and Notch signaling. *Science*, **342**, 734–737.
65. Song, M., Mihara, K., Chen, Y., Scorrano, L. and Dorn, G.W., 2nd (2015) Mitochondrial fission and fusion factors reciprocally orchestrate mitophagic culling in mouse hearts and cultured fibroblasts. *Cell Metab.*, **21**, 273–285.

66. Song, M., Franco, A., Fleischer, J.A., Zhang, L. and Dorn, G.W., 2nd (2017) Abrogating mitochondrial dynamics in mouse hearts accelerates mitochondrial senescence. *Cell Metab.*, **26**, 872–883.e875.
67. Zhou, Y., Carmona, S., Muhammad, A., Bell, S., Landeros, J., Vazquez, M., Ho, R., Franco, A., Lu, B., Dorn, G.W., 2nd et al. (2021) Restoring mitofusin balance prevents axonal degeneration in a Charcot-Marie-Tooth type 2A model. *J. Clin. Invest.*, **131**, e147307.
68. Zuchner, S., Mersiyanova, I.V., Muglia, M., Bissar-Tadmouri, N., Rochelle, J., Dadali, E.L., Zappia, M., Nelis, E., Patitucci, A., Senderek, J. et al. (2004) Mutations in the mitochondrial GTPase mitofusin 2 cause Charcot-Marie-Tooth neuropathy type 2A. *Nat. Genet.*, **36**, 449–451.
69. Verhoeven, K., Claeys, K.G., Zuchner, S., Schroder, J.M., Weis, J., Ceuterick, C., Jordanova, A., Nelis, E., De Vriendt, E., Van Hul, M. et al. (2006) MFN2 mutation distribution and genotype/phenotype correlation in Charcot-Marie-Tooth type 2. *Brain*, **129**, 2093–2102.
70. Feely, S.M., Laura, M., Siskind, C.E., Sottile, S., Davis, M., Gibbons, V.S., Reilly, M.M. and Shy, M.E. (2011) MFN2 mutations cause severe phenotypes in most patients with CMT2A. *Neurology*, **76**, 1690–1696.
71. Bombelli, F., Stojkovic, T., Dubourg, O., Echaniz-Laguna, A., Tardieu, S., Larcher, K., Amati-Bonneau, P., Latour, P., Vignal, O., Cazeneuve, C. et al. (2014) Charcot-Marie-Tooth disease type 2A, from typical to rare phenotypic and genotypic features. *JAMA Neurol.*, **71**, 1036–1042.
72. Zhang, L., Dang, X., Franco, A., Zhao, H. and Dorn, G.W. (2022) Piperine derivatives enhance fusion and axonal transport of mitochondria by activating mitofusins. *Chemistry*, **4**, 655–668.
73. Franco, A., Kitsis, R.N., Fleischer, J.A., Gavathiotis, E., Kornfeld, O.S., Gong, G., Biris, N., Benz, A., Qvit, N., Donnelly, S.K. et al. (2016) Correcting mitochondrial fusion by manipulating mitofusin conformations. *Nature*, **540**, 74–79.
74. Zacharioudakis, E., Agianian, B., Kumar Mv, V., Biris, N., Garner, T.P., Rabinovich-Nikitin, I., Ouchida, A.T., Margulets, V., Nordstrøm, L.U., Riley, J.S. et al. (2022) Modulating mitofusins to control mitochondrial function and signaling. *Nat. Commun.*, **13**, 3775.
75. Li, J., Dang, X., Franco, A. and Dorn, G.W. (2022) Reciprocal regulation of mitofusin 2-mediated mitophagy and mitochondrial fusion by different PINK1 phosphorylation events. *Front. Cell Dev. Biol.*, **10**, 868465.
76. Zhao, R.Z., Jiang, S., Zhang, L. and Yu, Z.B. (2019) Mitochondrial electron transport chain, ROS generation and uncoupling (Review). *Int. J. Mol. Med.*, **44**, 3–15.
77. Beaudet, M.J., Yang, Q., Cadau, S., Blais, M., Bellenfant, S., Gros-Louis, F. and Berthod, F. (2015) High yield extraction of pure spinal motor neurons, astrocytes and microglia from single embryo and adult mouse spinal cord. *Sci. Rep.*, **5**, 16763.